

A Simulation Benchmark for Vision-based Autonomous Navigation

Lauri Suomela¹, Atakan Dag¹, Harry Edelman¹, and Joni-Kristian Kämäriäinen¹

Tampere University {lauri.a.suomela, atakan.dag, harry.edelman, joni.kamarainen}@tuni.fi

Abstract. This work introduces a simulator benchmark for vision-based autonomous navigation. The simulator offers control over real world variables such as the environment, time of day, weather and traffic. The benchmark includes a modular integration of different components of a full autonomous visual navigation stack. In the experimental part of the paper, state-of-the-art visual localization methods are evaluated as a part of the stack in realistic navigation tasks. To the authors' best knowledge, the proposed benchmark is the first to study modern visual localization methods as part of a full autonomous visual navigation stack.

Keywords: Autonomous visual navigation, benchmark dataset

1 Introduction

One of the most impressive capabilities of the human brain is the ability to take a look around, answer the question "Where am I?", and use a mental map of the environment to guide one to the coffee room or any other desired place that has been visited before. A task that seems trivial to humans is notoriously difficult for robots. One promising approach to *autonomous navigation* is vision-based navigation that uses *visual localization* to estimate the pose of an agent with respect to a known environment. Visual localization is based on a "gallery set" of images captured from an environment. The location and pose of new "query images" is estimated by matching them to the gallery set. This process is illustrated in Figure 1. Much of the ongoing research on visual localization focuses on developing better methods that are more robust to viewpoint and appearance changes between the query and gallery images. In recent years, various benchmarking datasets for visual localization have been published [50,16,26], and visual localization challenges have been hosted as part of the top-tier computer vision conferences. The performance of the methods is measured by how close the estimated pose is to the true pose of an image. The new methods strive for more and more accurate results on the benchmark datasets.

The most common applications of visual localization that are mentioned in papers are autonomous driving and augmented reality [50,26]. However, none of the new deep learning based localization methods have been demonstrated as

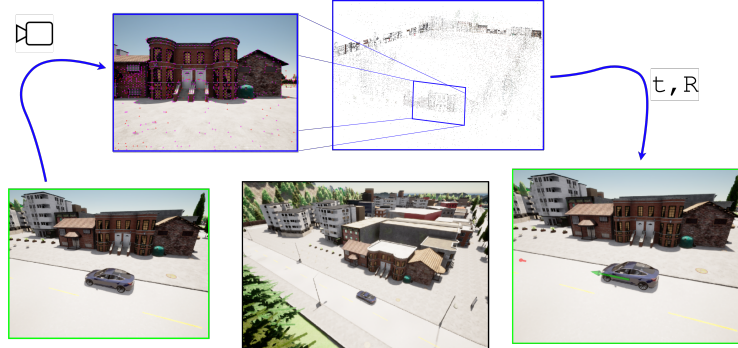


Fig. 1: Left to right: the vehicle finds its 6-DoF pose in a simulated environment by retrieving the best matching image in gallery and then matching local features to a pre-built 3D model. This enables vision-based autonomous navigation along known routes.

part of a robot navigation stack. This raises the question: how relevant are the performance metrics used by the visual localization benchmarks and challenges for autonomous navigation? And how accurate do the localization methods actually have to be in order to enable autonomous robot navigation?

This paper seeks to address these concerns. We present a simulator environment for testing visual localization methods for autonomous navigation. In the environment, the user can test how various state of the art methods for visual localization perform when they are used for guiding navigation of an autonomous car. This ability to directly test the performance of visual localization algorithms in their intended purpose enables the discovery of relevant new research problems, as compared to focusing on just measuring the accuracy of the localization algorithms. Using a simulator also enables experiments which study the effects of environmental factors such as illumination conditions, weather and dynamic objects on visual navigation. Furthermore, the use of a simulator enables comparing the output of the visual localization algorithms with the accurate ground truth location of the autonomous vehicle. When testing the methods with data collected from the real world, only pseudo ground truth information that is not completely accurate is available [6]. As pointed out by Brachmann *et al.* [6], synthetic data seems to be "easier" for a visual localization method to handle when compared to real camera data. Because of this, the navigation results reported in our work are likely to be overly optimistic. Even so, we argue that the ability to test an end-to-end visual navigation stack provides important new knowledge into the discussion on visual localization methods. Our main contributions are: **1)** A simulated benchmark which enables development and evaluation of components in a vision-based autonomous navigation stack for realistic navigation tasks; **2)** An example use-case of the benchmark: evaluation of the state-of-the-art visual localization methods as part of a navigation stack; **3)** Novel findings that connect a visual localization performance metric, recall rate, with a pro-

posed new metric for simulated autonomous navigation, failure rate. All results are fully reproducible and the benchmark will be made publicly available.

2 Related Work

This work focuses on *autonomous visual navigation* which can be used by autonomous mobile robots to handle various tasks such as delivery, inspection and people transportation [18,57]. Visual navigation is useful in conditions where GPS or other sensors such as LiDAR [40], external cameras [34] or active localization beacons [29] are not available or fail. The advantage of visual navigation is that it only requires commodity RGB cameras. The most common approaches are visual-inertial odometry (VIO) and visual simultaneous localization and mapping (SLAM). The two terms are sometimes utilized interchangeably: the methods are similar, but they focus on different parts of the visual perception problem. Visual SLAM is more popular in robotics community, but for robots moving along repetitive routes, rebuilding the full 3D map of the environment on each pass is not necessary for navigation. It is enough that a robot can localize itself within a previously built map.

Teach-&-repeat navigation. In the robotics literature, the type of navigation based on following a previously performed route is commonly referred to as teach-&-repeat (T&R) navigation [8]. In visual T&R navigation, an expert first drives a robot through a route. This is called the teach phase. During the teach phase, the robot captures photos along the route and stores them in a gallery database. Then, during the repeat phase, the robot is able to navigate along the same route independently by capturing new images and comparing them to the gallery images. Visual T&R has been utilized, for example, in planetary rovers [19], wheeled utility robots [39] and drones [38,58].

The visual T&R methods can be divided into two categories: *appearance-based* and *geometric* [8]. The appearance based methods directly translate the camera input into robot control commands, without the need of building an explicit map-representation of the environment. However, this kind of navigation is not robust, as the failure to reach a single intermediate goal can lead to the failure of the whole route-following method [12]. The geometric methods rely on a map which represents the environment. The robot captures images from its surroundings, and uses the images to deduce its position and orientation with respect to the map. This problem is referred to as *visual localization*.

Visual localization. There are various approaches to visual localization, such as pose regression [25], scene coordinate regression [54] and direct image alignment [56,49], but in recent years *hierarchical localization* [23,47] methods have dominated the benchmarks. Similar to visual T&R, hierarchical localization requires an image database representing the known environment and referred as "gallery set". New images, called "query images", are localized by comparing them to the gallery set. The comparison consists of two stages. First, the gallery

images that are most similar to the query image are retrieved using place recognition methods [59]. Then, the local features from the query image and the best matching gallery images are matched to determine the correspondences between the query image and the environment 3D structure. Based on these 2D to 3D correspondences, the 6-DoF pose of the query image is estimated using Perspective-n-Point (PnP) methods [20]. The hierarchical visual localization approach has proven to be robust to changes in viewpoint and appearance, and is computationally feasible even for large-scale environments [47]. For a comprehensive survey on place recognition methods for prior retrieval we refer the reader to [33]. A similar review of local feature descriptors and descriptor matching is presented by Ma *et al.* [28]. One of the characteristics of autonomous navigation which is relevant for the design of visual localization systems is the sequential nature of the image data that the vehicle cameras capture. A vehicle cannot teleport. Instead, it is moving through space in a continuous manner. This prior information can be utilized at different stages of the hierarchical localization pipeline. In the prior retrieval step of hierarchical localization, the prior can be employed by retrieving best matching image descriptor sequences instead of individual images [35,37], by creating descriptors representing whole image sequences [21] or by using the current pose estimate as a prior for topological localization [55]. At the local feature matching stage, an image sequence can be modelled as a generalized camera [41], which enables estimating the camera trajectory from multiple images simultaneously [55]. Another approach is to add sequential processing on top of the visual localization outputs. Filtering and smoothing based methods can be used for rejecting erroneous pose estimates, helping to recover the likely trajectory of the vehicle. Kalman filters [7], particle filters [1] and graph-based methods [38,58] have been utilized for such purposes. The pose-level processing also enables fusion of the visual localization output with other sensing modalities, improving the stability of vision-based navigation in challenging conditions.

Benchmarks. To the authors' best knowledge the proposed simulator benchmark is the first dynamic benchmark where the components of visual navigation stack can be individually developed and evaluated in fair and reproducible manner. The other benchmark options are static sets of real or synthetic images for which visual localization recall can be computed but its contribution to visual navigation remains unclear. Real world datasets include, for example, Aachen Day-Night [50], Oxford RobotCar [30], CMU VL [4] and Visual Localization Benchmark (VLB) [50]. Real world datasets provide pseudo ground truth computed from SfM or LiDAR reconstruction. SimLocMatch [5] is a synthetic dataset collected for the CVPR 2021 Workshop on Image Matching. V4RL [31] is a hybrid dataset where images and ground truth are obtained synthetically, but the environment is a photogrammetric reconstruction of real world images.

Table 1: Factors that can have impact on visual navigation performance and that are / aren’t supported by our benchmark and demonstrated in this paper.

F# Factor	Possible	Reported	F# Factor	Possible	Reported
F1 Time of day (illumination)	✓	✓	F6 Camera placement (extr.)	✓	✗
F2 Weather	✓	✗	F7 Multiple cameras	✓	✗
F3 Time of year (seasons)	✗	✗	F8 Scene texture & structure	✓	✗
F4 Viewpoint changes	✓	✗	F9 Dynamic objects	✓	✗
F5 Camera parameters (intr.)	✓	✗	F10 Headlights	✓	✗

3 Simulation Benchmark

Based on the discussion in Sec. 2, we identified the research gap between visual localization and visual navigation research. Visual localization is an active research topic in computer vision, but methods are evaluated using static datasets and it is unclear how well the methods would work as a part of the visual navigation stack, where visual localization output would be used for closed-loop control. As a solution we present a benchmark which enables easy experimentation with different visual localization methods as part of visual navigation. The platform enables investigating various important performance factors of visual localization based autonomous navigation, for example those listed in Tab. 1.

The benchmark is based on the Carla autonomous driving simulator [14] and a ROS2 [32] port of the Hloc visual localization toolbox [46]. Carla was chosen because of its simplicity of use, relatively high level of photorealism and ROS2 support via the Carla ROS bridge module. ROS2 enables easy integration of the demonstrated visual localization package with different robotic platforms.

3.1 ROS2 Visual localization package

In order to provide a generic visual localization interface to autonomous agents, we created the *ROS2 Visual Localization Package* (ROS2-VLP). The package is a wrapper for the Hloc toolbox [46] that is a collection of state-of-the-art visual localization methods and utility functions. Hloc utilizes the Colmap SfM library [51,53] for retrieving the 3D structure of the scenes represented by the gallery set. The original toolbox is designed for static gallery and query sets, but our ROS2-VLP extends it to images arriving in a real-time stream.

The ROS2-VLP workflow is as follows. First, a gallery set is collected for each test environment. Inside the simulator this is achieved by driving a reference run with Carla’s built-in autopilot. Along the route, images are captured by a camera attached to the vehicle. The images are taken at steady intervals, and saved to disk along with the exact camera pose. After the gallery set has been captured, the images are processed to extract global and local feature descriptors. These are saved in a gallery database for queries. The 3D locations of the extracted local features are then estimated with Colmap. Instead of running full SfM reconstruction we use point triangulation from known camera poses [22]. This produces higher quality 3D scene models than reconstructions from un-ordered collections of images. In the simulator, acquiring the exact camera poses

is trivial. In the real world, LiDAR SLAM methods can be employed in the mapping phase to ensure high-fidelity 3D models [9,26].

At inference time, the vehicle captures a query image which is sent to ROS2-VLP for pose estimation. First, a global descriptor is extracted from the image for prior retrieval. The descriptor is compared to those of the gallery images, and the images with the most similar descriptors are retrieved. The retrieved gallery images are divided into distinct groups according to the parts of the scene 3D model they are observing using co-visibility clustering [47]. Then, local descriptors are extracted from the query image, and these are matched with the local features of the retrieved gallery images. Since the 3D locations of the local features from the gallery images are known, this enables acquiring the 2D-3D correspondences of the query local features. The 2D-3D correspondences are used as inputs to the Perspective-n-Point (PnP) [20] solver provided by Colmap to produce 6DoF pose estimates for each cluster. The PnP solver includes a geometric consistency check using RANSAC to filter outliers [17]. The estimated pose from the cluster with the highest number of inlier 2D-3D correspondences is chosen as the final output of the visual localization pipeline. This pose estimate is forwarded to the *vehicle’s motion planning and control stack* where it is used for producing steering commands.

Hloc includes various localization method options. There are two global descriptor methods, NetVLAD [3] and Ap-GeM [44], which we test in conjunction with the four supported local feature extractors, SIFT [27], D2-net [15], R2D2 [45] and SuperPoint [13]. With all methods besides SuperPoint we conduct the local feature matching by nearest neighbor search with ratio test [28] (NN-ratio). With SuperPoint, we utilize the SuperGlue matcher [48] instead.

3.2 Vehicle motion planning & control components

In addition to ROS2-VLP for visual localization, the navigation stack needs two more components: *a motion planner* and *a controller*. Motion planner is sub-divided into *global* and *local planners*. Based on a route description, a global planner produces a set of waypoints from the vehicle’s start position to its target. It is used in combination with a local planner. The local planner takes the vehicle’s current pose estimate and the global planner’s waypoints as input. At each time step, the local planner finds the waypoint closest to the current pose, which is passed on to a controller. The controller consists of two proportional-integral-derivative (PID) controllers [2], one for longitudinal and one for lateral control of the vehicle. Its purpose is to produce steering commands to move the vehicle towards the waypoint from local planner. The global planner and controller of our stack are the standard ones included in the Carla ROS bridge. The local planner we implemented ourselves.

Sensor fusion & sequential processing. The pose estimates of the ROS2-VLP visual localization package, however, are not directly passed to the local planner or controller. Instead, the estimates are first forwarded to a Kalman filter,

which fuses the visual localization output with linear and angular velocity estimates from a simulated wheel odometry sensor. The true values from the ideal odometry are injected with gaussian noise to make the sensor more realistic. The reason we fuse the visual pose estimates with wheel odometry data is that the PID-controller of the vehicle requires pose input at a high frequency, which is not achievable with the current state-of-the-art hierarchical visual localization systems. The wheel odometry also enables the vehicle to get estimates of its position when the environment is so degraded that the PnP solver of the visual localization pipeline cannot converge to a solution. In theory, vehicle could navigate using pose information from wheel odometry alone. But as the odometry measurements contain noise, the estimated pose accumulates noise over time. This drift limits wheel odometry navigation only for short distances. Fusing the wheel odometry with visual localization effectively corrects the drift. We use the extended Kalman filter (EKF) implementation of the `robot_localization` ROS package [36]. To make the localization system more robust to outliers, visual pose estimates with more than 20 meters deviation from the filter's current state are discarded. This scheme addresses the sequential nature of visual localization in autonomous navigation context at the pose level, and introduces a degree of temporal stability to the pose estimates.

An error source present in this design is the computation delay of the visual localization. Our vehicle is moving, so the pose estimate for an image captured at certain position is available after a short delay. When the result pose estimate is input to the Kalman filter, its state will be corrected towards the pose where the image was taken, not towards the vehicle's actual pose after the computation delay. Graph-based smoothers could cope with delayed measurements [52]. Implementing these, however, we leave for future work.

3.3 Evaluation scheme and performance metrics

Perhaps the most important part of any benchmark system is the performance measurement. In this work, we wanted to bring together visual localization and visual navigation to serve both computer vision and autonomous robotics research, and therefore metrics should be meaningful to the both. Autonomous driving oriented visual localization performance metrics such as "probability distribution of certain distance driven without localization" [42] and "maximum open loop distance" [11] have been proposed, but whether they indicate success in autonomous navigation or have been invented to circumvent limitations of static datasets is unclear. The autonomous driving performance is often measured with the vehicle's deviation from a reference trajectory or lane center line [43], but this is conditional to that no crashes occur, which is essential with real vehicles but not in simulations.

Our performance measures are inspired by visual object tracking (VOT) research where performance evaluation methodologies have been investigated rigorously. We observe that many of the insights from VOT can be transferred to visual navigation with small modifications: in both fields, the essence is in measuring how well a system can estimate the pose of an object in its environment.

The works of Kristan *et al.* [24] and Cehovin *et al.* [10] describe the performance measurement methodology of the influential VOT challenge, and provide a thorough analysis of the different metrics. In accordance with their results, we adopt two metrics describing the *accuracy* and *robustness* of navigation.

Recall rate. The first aspect of performance is the accuracy of the visual localization method. This is an intuitive measure of how well a visual localization method performs under different conditions. For each experiment environment we conduct a test where a vehicle drives through the test route with visual localization running. However, to produce comparable measurements of the accuracy of the visual localization methods, we don't their output for navigation, but only measure its accuracy. For navigation the vehicle uses ground truth pose information from the simulator. Navigating based on the visual localization estimates, which can contain large errors, would lead to the vehicle driving a bit different route on each test run, affecting the repeatability of the accuracy measurements. For each combination of experiment settings and localization methods we report the *localization recall*, which was adopted from visual localization benchmark of Sattler *et al.* [50]. We report the proportion of correct poses within three error thresholds: $< 0.25\text{m}$, 2° (T1), $< 0.5\text{m}$, 5° (T2) and $< 5\text{m}$, 10° (T3). The distance of the estimated pose is compared to the pose of the vehicle at the moment the visual localization input image was taken.

Failure rate. The recall rate of a localization method doesn't fully describe its performance in autonomous driving context. A high accuracy value can conceal infrequent but catastrophically large localization failures, which cause the vehicle to crash. Thus, to complement the accuracy metric, we measure the robustness of the full autonomous driving stack. To evaluate it, a vehicle is set to drive a predefined route while localizing based on sensor data. If localization error causes the vehicle to crash, the vehicle and its EKF state are re-initialized back to the point along the route where it got lost. The re-initialization enables evaluating the localization performance along all segments of the test route: without it, the test sequence would be ended by a crash caused by the first difficult segment of the route. Similar to VOT [24,10], we report the *failure rate* of navigation

$$F = \frac{N_{reinit}}{L_{path}} , \quad (1)$$

where N_{reinit} is the number of re-initializations needed to complete a path, and L_{path} is the length of the path in kilometers. Since the autonomy stack of the vehicle is effectively using the visual localization to correct the wheel odometry drift *i.e.* to improve navigation performance from that of a wheel odometry only based system, we also measure the performance of a vehicle navigating using wheel odometry only. This defines a '*baseline*' to which the autonomy stack with visual localization should be compared. In easy conditions, the visual localization can be expected to improve navigation performance, while in degraded conditions the estimates can be very wrong and actually make it worse. Because

of the stochastic nature of the navigation, we repeat the robustness experiments multiple times for each test condition and report the average failure rate.

4 Experiments

To demonstrate the capabilities of the proposed simulator benchmark we performed experiments to compare the ability of different visual localization methods to cope with gallery-to-query appearance change, as produced by changes in scene illumination. Although we conducted experiments on appearance change only, we want to emphasize that the proposed system can be just as easily utilized to experiment with other factors of interest, e.g, those listed in Tab. 1.

We limit our experiments to the state-of-the-art hierarchical localization methods, and do not consider other approaches such as direct image alignment [56,49]. For experiments where the query-to-gallery appearance change is larger than the corresponding change in viewpoint, other types of visual localization could perform as well or better than the hierarchical methods. However, we leave the integration of other method families for future work.

4.1 Illumination change

This experiment evaluated the performance of the state-of-the-art visual localization methods under illumination change. Two different Carla environments were used in the experiments, "Town01" and "Town10" (Fig. 2). The gallery sets were gathered by driving around the towns in mid-day sunny conditions and capturing images every 2 meters by a camera pointed perpendicular to the right of the vehicle's direction of travel. At test time, the autonomous vehicle attempts to follow the same route using pose estimated from sensor data.

Environments. Out of the 8 ready-made default maps in Carla we selected two that represent two very different environments. Town01 is a model of a small town with densely packed buildings and a river in the center. We defined a 1.2-kilometer long test route, from which a gallery set of 615 images was produced. The route consists of straight road segments connected by five 90 degree turns. Town10 is a part of a bigger city with large buildings, skyscrapers and a beach. The route is approximately 0.5 kilometer long with six turns. The captured gallery has 237 images.

Methods and parameters. Each of the localization methods included in Hloc (see Sec. 3.1) was tested in both of the environments. None of the methods were retrained with data from the simulator; pretrained model weights were acquired from the original Github repositories. The number of gallery images retrieved by place recognition for 6DoF pose estimation was set to 5. Ratio threshold of NN-ratio matcher was set to 0.8, and SuperGlue was used with the default parameters. For all of the localization methods we used input image resolution of 800x600 pixels. The target speed of the vehicle and the localization frequency

were set to $4m/s$ and $2Hz$, respectively. Magnitude of the wheel odometry noise was set to a level which causes the pose estimated to drift away from the true pose at a rate of 8.5% for the position and $0.4^\circ/m$ for the orientation.

Daylight illumination control. The autonomous vehicle was set to perform the test routes under multiple illumination conditions (Fig. 3). In the easiest test scenario the illumination corresponds to that of the gallery set, and in the most difficult scenarios there is almost complete darkness. To determine the failure rate metric, the route was repeated 5 times with each combination of a localization method and illumination condition. We report the average failure rate from these runs. For the visual localization recall rate, we only report the results from one run per test condition since the vehicle drives using error-free controller and therefore the variance between the runs is negligible.

In Carla, illumination is controlled by two parameters: sun intensity and sun elevation angle. These two have to be adjusted jointly to produce a full range of illumination conditions from daylight to darkness. We start from sun intensity value of 1.0 and elevation angle $0.4\pi rad$, and for each successive illumination condition we halve the values from the previous condition by parameter k in the following way:

$$V_k = V_{base} * 0.5^k \quad (2)$$

where V_{base} is sun intensity or elevation angle value for the gallery set, and V_k is the elevation angle or intensity for illumination condition k . $k \in [0, 1, \dots, 10]$ leads to 11 distinct illumination conditions. See Figure 3 for illustrations.

In addition to the failure and localization recall rates in Sec. 3.3, we also report the average computation times for the different visual localization methods. This enables estimating the pose error caused by delays in estimated poses (see Sec. 3.2).

5 Results and Discussion

Method comparison. The recall rates for visual localization are in Table 3 and navigation failure rates for autonomous visual navigation in Table 2 and Fig. 4.

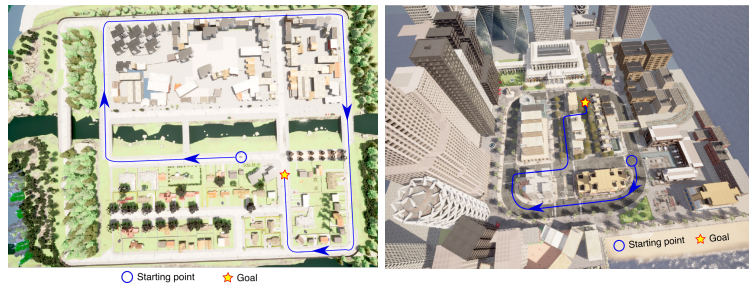


Fig. 2: A bird's-eye view of the test routes in Town01 (left) and Town10 (right)

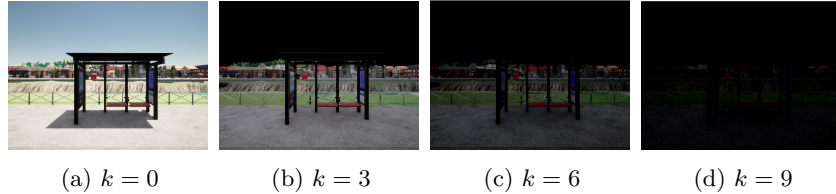


Fig. 3: Images from "Town01" environment under different illumination conditions, each characterized by its k -value.

Table 2: Autonomous visual navigation failure rates over 5 repeated runs of the same route in each daylight illumination level k conditions. Smaller is better. The last column (\dagger) presents the computation time for each method in milliseconds.

		Town01										Town10										\dagger		
		$k = 0$	1	2	3	4	5	6	7	8	9	10	0	1	2	3	4	5	6	7	8	9	10	
Ap-GeM	Sift	0.8	3.0	6.8	5.0	6.5	7.6	12.9	30.1	34.2	28.5	25.2	0.9	0.9	2.2	3.1	3.6	4.0	8.9	21.9	33.0	27.2	23.7	241
	D2-net	0.7	6.8	12.6	14.4	13.6	14.4	23.0	27.8	23.2	21.0	20.7	0.0	4.9	6.7	5.8	6.2	9.8	16.5	15.6	12.1	11.2	11.6	205
	R2D2	0.0	1.8	3.8	4.0	5.0	6.0	8.1	18.0	22.4	21.2	18.2	0.0	2.7	5.8	6.2	5.8	5.8	11.6	12.9	18.3	13.4	12.9	218
	SuperPoint	0.7	0.5	0.3	0.5	0.3	0.5	0.7	3.1	7.6	15.1	19.2	1.8	4.0	3.6	2.7	2.7	3.6	4.5	4.0	6.2	11.2	15.2	226
NetVLAD	Sift	0.2	2.0	5.8	6.8	5.8	7.3	12.3	29.0	30.8	27.8	23.8	0.0	0.9	2.7	4.0	3.1	1.3	11.6	18.3	33.5	31.2	25.0	209
	D2-net	0.7	8.1	14.6	12.9	11.8	16.2	24.0	27.6	23.2	22.5	19.0	0.0	3.1	3.6	4.5	6.2	7.6	19.2	21.4	11.6	14.3	11.6	202
	R2D2	0.2	0.8	3.1	4.5	5.0	5.0	9.6	16.7	19.2	19.4	21.2	0.0	0.0	3.6	4.9	4.5	2.7	6.2	15.2	20.1	11.2	14.7	192
	SuperPoint	0.0	0.2	0.3	0.2	0.0	0.0	0.3	1.5	4.5	11.9	17.9	0.0	0.9	1.8	0.4	1.8	1.8	0.9	4.0	8.9	8.5	207	
Wheel odom		18.5											10.7											

The combination of NetVLAD, SuperPoint and SuperGlue, is the best performing method on the both metrics and by clear margin. The second best performing combination is the one where NetVLAD is replaced with Ap-GeM. This follows a general pattern: The local feature method seems to have more effect on the performance than the place retrieval method. Of the two place recognition methods NetVLAD consistently provides a slightly better performance. The ranking of the local features is (from best to worst): SuperPoint, R2D2, SIFT, D2. It is interesting to see that D2, a newer deep learning based feature, performs worse than the age-old SIFT.

Autonomous navigation failure rates. Important findings for autonomous visual navigation can be obtained from Fig. 4. The failure rates steadily increase while the illumination defined by k gets dimmer. When the test time illumination corresponds to the gallery set, $k = 0$, the failure rate is close to 0. Most of the methods reach their peak failure rate around k -value 7 or 8. Around the peak, the gallery-to-query appearance change is large enough to cause big errors in the visual localization. However, these aren't big enough to cause rejection by the EKF 20m outlier rejection threshold, so they affect the filter pose estimate. When the illumination further decreases ($k = 9, 10$) the deviation of the visual pose estimates becomes so large that most of the estimates are rejected by the filter, and the vehicle mostly relies on wheel odometry. Thus, the failure rate decreases and converges towards the failure rate of wheel odometry only. In this regard, the ability of SuperPoint and SuperGlue to improve navigation performance is

Table 3: The visual localization recall rates for the reference paths. The accuracy thresholds used are T1 ($\leq 0.25m$, $\leq 2^\circ$), T2 ($\leq 0.50m$, $\leq 5^\circ$) and T3 ($\leq 5.00m$, $\leq 10^\circ$). Full table for all illumination levels k in the supplementary material.

		$k = 0$	2	4	6	8	10
		T1 / T2 / T3	T1 / T2 / T3	T1 / T2 / T3	T1 / T2 / T3	T1 / T2 / T3	T1 / T2 / T3
Town01	Ap-GeM	Sift 96.4 / 97.0 / 98.0	83.7 / 87.3 / 94.9	82.4 / 85.0 / 92.3	69.2 / 73.1 / 85.3	19.8 / 23.5 / 30.6	3.6 / 4.7 / 8.8
	D2-net	92.6 / 95.6 / 99.5	70.5 / 77.2 / 90.8	69.7 / 75.8 / 89.3	46.9 / 56.4 / 75.7	9.3 / 12.3 / 16.4	0.8 / 1.3 / 2.3
	R2D2	95.2 / 97.2 / 99.0	82.7 / 88.7 / 96.2	81.6 / 86.0 / 97.0	72.2 / 79.4 / 92.0	27.6 / 34.0 / 44.7	9.2 / 12.2 / 14.0
	SuperPoint	99.2 / 99.2 / 99.2	97.0 / 98.0 / 98.0	96.9 / 97.9 / 97.9	93.6 / 94.7 / 94.9	67.3 / 72.5 / 77.6	35.5 / 38.8 / 47.0
NetVLAD	Ap-GeM	Sift 95.7 / 97.2 / 99.0	87.0 / 91.3 / 98.0	85.9 / 90.0 / 96.2	71.6 / 79.0 / 90.6	22.1 / 25.7 / 34.5	4.9 / 7.2 / 12.0
	D2-net	94.1 / 95.9 / 99.8	68.8 / 77.0 / 91.2	69.7 / 76.3 / 89.3	48.7 / 57.1 / 77.6	9.6 / 12.3 / 16.2	0.5 / 0.8 / 2.6
	R2D2	94.4 / 96.9 / 99.8	81.0 / 87.4 / 97.4	80.5 / 86.0 / 96.6	74.1 / 81.0 / 93.8	33.1 / 37.2 / 49.9	12.3 / 14.3 / 16.8
	SuperPoint	99.8 / 99.8 / 99.8	98.8 / 99.3 / 99.7	98.5 / 99.2 / 99.5	97.5 / 98.2 / 98.4	69.8 / 75.1 / 79.7	39.7 / 44.3 / 51.1
Town10	Ap-GeM	Sift 94.4 / 98.4 / 99.6	89.6 / 91.2 / 92.8	90.1 / 91.3 / 93.3	72.8 / 76.8 / 81.5	11.2 / 15.7 / 30.9	0.0 / 1.6 / 4.0
	D2-net	98.0 / 99.6 / 100.0	87.2 / 90.4 / 93.2	82.1 / 86.5 / 92.1	47.6 / 58.8 / 66.4	0.0 / 0.0 / 0.8	0.0 / 0.0 / 0.0
	R2D2	87.3 / 90.4 / 99.6	90.5 / 92.1 / 92.9	84.0 / 85.6 / 91.6	74.6 / 76.6 / 83.3	13.2 / 18.0 / 27.6	0.0 / 0.8 / 1.6
	SuperPoint	98.4 / 98.8 / 99.2	95.6 / 96.4 / 96.4	96.0 / 96.0 / 96.8	92.8 / 93.2 / 94.2	64.7 / 66.3 / 67.1	30.6 / 33.7 / 36.5
NetVLAD	Ap-GeM	Sift 94.9 / 97.2 / 98.8	94.4 / 94.8 / 96.0	88.8 / 90.8 / 92.4	79.1 / 84.7 / 88.0	13.6 / 19.2 / 36.0	0.4 / 0.4 / 2.4
	D2-net	97.2 / 99.2 / 100.0	87.3 / 90.8 / 94.4	84.4 / 89.2 / 93.6	44.8 / 54.4 / 67.1	0.0 / 0.0 / 0.8	0.0 / 0.0 / 0.4
	R2D2	90.4 / 93.6 / 99.2	88.8 / 90.0 / 94.4	86.9 / 89.2 / 93.2	78.5 / 81.7 / 88.0	13.5 / 18.7 / 30.6	0.4 / 1.2 / 2.8
	SuperPoint	99.6 / 100.0 / 100.0	98.0 / 98.4 / 97.6	97.6 / 98.0 / 96.8	70.3 / 71.9 / 73.1	40.9 / 42.1 / 45.2	

remarkable. Combined with NetVLAD, the method brings benefits over wheel odometry even at $k = 10$, when localizing the images is very difficult for even the human eye.

The failure rates from the two towns exhibit some differences. In Town01, SuperPoint has significantly better performance than the other methods. In Town10, this gap is narrower. This is likely caused by higher degree of perceptual aliasing in Town10 scene. Along the route, a building with repetitive structure is observed from various perspectives, causing localization failures. However, in both environments the overall order of method performance remains more or less the same - only R2D2 and SIFT switch places on some k -values.

Visual localization recall vs. navigation failures. An important question is the extent to which the visual localization performance metric, recall, measures suc-

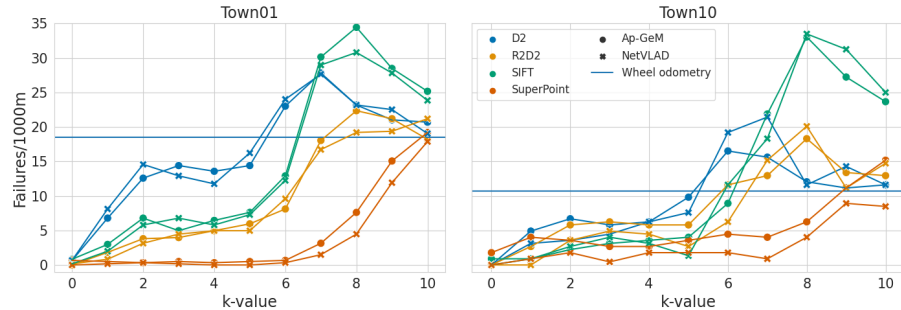


Fig. 4: Relationship between failure rate and illumination level. Marker color indicates type for local features, shape for global features.

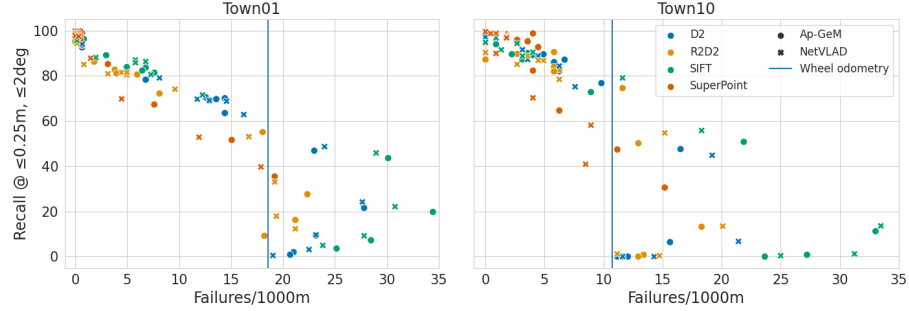


Fig. 5: Relationship between the failure rate and recall rate T1 ($\leq 0.25\text{m}$, $\leq 2^\circ$) for both towns. Marker color indicates type for local features, shape for global features.

cess in autonomous navigation. Fig. 5 shows the correlation plot between the two metrics and over all illumination conditions. As expected, they are strongly correlated, but the plots also provide two important findings: **1)** SuperPoint, that achieves the lowest failure rates in different illumination conditions, also achieves the lowest failure rate for a given recall rate; **2)** there is a certain operation point after which changes in the recall rate become meaningless for autonomous navigation. Especially the second finding is novel and interesting as it shows that visual localization performance needs to be sufficiently good in order to improve over wheel odometry only. For Town01 and the tightest recall threshold (T1) only recall rates above 60% improve navigation. In other words, improving from 40% to 50% is almost meaningless while from 60% to 70% is clearly significant. For Town10 this operation point is even higher and improvements should focus on 80% and above. This is intuitive, but not possible to observe from recall rates on static datasets. The critical operation point in the both cases is related to the performance point of navigation with wheel odometry only.

Spatial distribution of navigation failures. The first consequence of illumination decrease is that the vehicle starts to crash in certain parts of the route which contain 'difficult' scene structures (perceptually aliased objects *etc.*). As the k -value is increased, the visual pose estimates become erroneous everywhere along the route, leading to a more uniform distribution of crashes. The failure rate metric describes how often navigation failures happen, but it doesn't describe *where* the failures happen. The simulator enables visualization of the failure locations. Fig. 6 presents a screen capture of the simulator with crash locations for NetVLAD + R2D2 marked in red. Illustrations such as this are helpful for identifying structures and objects that are difficult for the visual localization algorithms. In the bottom close-up, for example, two almost identical buildings appear on the both sides of the road turn.



Fig. 6: Crash sites (red marks) of Town01 with NetVLAD+R2D2 and $k = 5$ (top left) and $k = 8$ (top right). Bottom figure is the closeup of a difficult route segment in the top left image, marked by a red rectangle.

Method runtimes. The failure rates Table 2 also includes the average runtime of the visual localization pipeline with each method, measured from Town10. At target velocity $4m/s$, these correspond to delay-induced positional errors in the range $[0.77, 0.96]$ meters. The error, however, is mostly in the longitudinal direction that doesn't seem to drastically affect navigation performance. During turns, the effect is more dominant.

6 Conclusion

This paper introduced a simulator benchmark for testing and developing different components of a visual navigation stack in reproducible way. To exemplify the benchmark we evaluated popular visual localization methods as a part of a vision-based autonomous navigation stack. The experiments on robustness of the methods to gallery-to-query appearance change demonstrated that the navigation failure rate metric can reveal information about the visual localization methods that is not observable from the traditional metrics such as localization recall alone. Substantial differences were observed in the performances of the methods, and it is clear that some methods are more suited to vision-based navigation than others. The presented benchmark enables studying the interaction of visual localization methods with robot planning and control algorithms. The results show that the naive controller used requires highly accurate position estimates from the visual localization method in order to succeed at navigation tasks. In the future, the benchmark could be used for studying the performance

gap between single-image and sequential visual localization, or for conducting experiments on the performance effects of factors such as gallery-to-query viewpoint change among others (Table 1). We hope that the research community finds the proposed benchmark useful for finding new, exciting research problems.

Limitations. Synthetic data is easier than real photos for many feature extractors. The simulator used in this paper does not incorporate all of the variation present in real world data. As such, the navigation results reported in this paper do not directly transfer into real robots.

Acknowledgements. This work was supported by a grant from the Technology and Innovation Institute (TII).

References

1. Akai, N., Morales, L.Y., Murase, H.: Simultaneous pose and reliability estimation using convolutional neural network and Rao–Blackwellized particle filter. *Advanced Robotics* **32**(17), 930–944 (2018), DOI: 10.1080/01691864.2018.1509726
2. Ang, K.H., Chong, G., Li, Y.: PID control system analysis, design, and technology. *IEEE Transactions on Control Systems Technology* **13**(4), 559–576 (Jul 2005), DOI: 10.1109/TCST.2005.847331
3. Arandjelović, R., Gronat, P., Torii, A., Pajdla, T., Sivic, J.: NetVLAD: CNN Architecture for Weakly Supervised Place Recognition. *IEEE Transactions on Pattern Analysis and Machine Intelligence* **40**(6), 1437–1451 (Jun 2018), DOI: 10.1109/TPAMI.2017.2711011
4. Badino, H., Huber, D., Kanade, T.: Real-time topometric localization. In: 2012 IEEE International Conference on Robotics and Automation. pp. 1635–1642 (May 2012), DOI: 10.1109/ICRA.2012.6224716, iSSN: 1050-4729
5. Balntas, V., Mishkin, D.: simlocmatch-benchmark (Aug 2021), <https://github.com/simlocmatch/simlocmatch-benchmark>, original-date: 2021-05-15T20:52:18Z
6. Brachmann, E., Humenberger, M., Rother, C., Sattler, T.: On the Limits of Pseudo Ground Truth in Visual Camera Re-localisation. arXiv:2109.00524 [cs] (Sep 2021), <http://arxiv.org/abs/2109.00524>, arXiv: 2109.00524
7. Brosh, E., Friedmann, M., Kadar, I., Lavy, L.Y., Levi, E., Rippa, S., Lempert, Y., Fernandez-Ruiz, B., Herzig, R., Darrell, T.: Accurate Visual Localization for Automotive Applications. In: 2019 IEEE/CVF Conference on Computer Vision and Pattern Recognition Workshops (CVPRW). pp. 1307–1316. IEEE, Long Beach, CA, USA (Jun 2019), DOI: 10.1109/CVPRW.2019.00170, <https://ieeexplore.ieee.org/document/9025353>
8. Camara, L.G., Pivoňka, T., Jílek, M., Gäbert, C., Košnar, K., Přeučil, L.: Accurate and Robust Teach and Repeat Navigation by Visual Place Recognition: A CNN Approach. In: 2020 IEEE/RSJ International Conference on Intelligent Robots and Systems (IROS). pp. 6018–6024 (Oct 2020), DOI: 10.1109/IROS45743.2020.9341764, iSSN: 2153-0866
9. Caselitz, T., Steder, B., Ruhnke, M., Burgard, W.: Monocular camera localization in 3D LiDAR maps. In: 2016 IEEE/RSJ International Conference on Intelligent Robots and Systems (IROS). pp. 1926–1931. IEEE, Daejeon, South Korea (Oct 2016), DOI: 10.1109/IROS.2016.7759304, <http://ieeexplore.ieee.org/document/7759304>
10. Cehovin, L., Leonardis, A., Kristan, M.: Visual object tracking performance measures revisited. *IEEE Transactions on Image Processing* pp. 1–1 (2016), DOI: 10.1109/TIP.2016.2520370, <http://ieeexplore.ieee.org/document/7389405/>
11. Clement, L., Gridseth, M., Tomasi, J., Kelly, J.: Learning Matchable Image Transformations for Long-Term Metric Visual Localization. *IEEE Robotics and Automation Letters* **5**(2), 1492–1499 (Apr 2020), DOI: 10.1109/LRA.2020.2967659
12. Dall’Osto, D., Fischer, T., Milford, M.: Fast and Robust Bio-inspired Teach and Repeat Navigation. In: 2021 IEEE/RSJ International Conference on Intelligent Robots and Systems (IROS). pp. 500–507 (Sep 2021), DOI: 10.1109/IROS51168.2021.9636334, iSSN: 2153-0866
13. DeTone, D., Malisiewicz, T., Rabinovich, A.: SuperPoint: Self-Supervised Interest Point Detection and Description. In: 2018 IEEE/CVF Conference on Computer Vision and Pattern Recognition Workshops (CVPRW). pp. 337–33712 (Jun 2018), DOI: 10.1109/CVPRW.2018.00060, iSSN: 2160-7516

14. Dosovitskiy, A., Ros, G., Codevilla, F., Lopez, A., Koltun, V.: CARLA: An Open Urban Driving Simulator. In: Proceedings of the 1st Annual Conference on Robot Learning. pp. 1–16. PMLR (Oct 2017), <https://proceedings.mlr.press/v78/dosovitskiy17a.html>, iSSN: 2640-3498
15. Dusmanu, M., Rocco, I., Pajdla, T., Pollefeys, M., Sivic, J., Torii, A., Sattler, T.: D2-Net: A Trainable CNN for Joint Description and Detection of Local Features. In: Proceedings of the IEEE/CVF Conference on Computer Vision and Pattern Recognition. pp. 8092–8101 (2019), https://openaccess.thecvf.com/content_CVPR_2019/html/Dusmanu_D2-Net_A_Trainable_CNN_for_Joint_Description_and_Detection_of_CVPR_2019_paper.html
16. ETH Zurich Computer Vision Group and Microsoft Mixed Reality \& AI Lab Zurich: The ETH-Microsoft Localization Dataset (Oct 2021), <https://github.com/cvg/visloc-iccv2021>, original-date: 2021-08-23T12:47:27Z
17. Fischler, M.A., Bolles, R.C.: Random sample consensus: a paradigm for model fitting with applications to image analysis and automated cartography. Communications of the ACM **24**(6), 381–395 (Jun 1981), DOI: 10.1145/358669.358692
18. Floreano, D., Wood, R.J.: Science, technology and the future of small autonomous drones. Nature **521**(7553), 460–466 (May 2015), DOI: 10.1038/nature14542, <https://www.nature.com/articles/nature14542>
19. Furgale, P., Barfoot, T.: Stereo mapping and localization for long-range path following on rough terrain. In: 2010 IEEE International Conference on Robotics and Automation. pp. 4410–4416 (May 2010), DOI: 10.1109/ROBOT.2010.5509133, iSSN: 1050-4729
20. Gao, X.S., Hou, X.R., Tang, J., Cheng, H.F.: Complete solution classification for the perspective-three-point problem. IEEE Transactions on Pattern Analysis and Machine Intelligence **25**(8), 930–943 (Aug 2003), DOI: 10.1109/TPAMI.2003.1217599
21. Garg, S., Milford, M.: SeqNet: Learning Descriptors for Sequence-Based Hierarchical Place Recognition. IEEE Robotics and Automation Letters **PP**, 1–1 (2021), DOI: 10.1109/LRA.2021.3067633
22. Hartley, R., Zisserman, A.: Multiple View Geometry in Computer Vision. Cambridge University Press, Cambridge, 2 edn. (2004), DOI: 10.1017/CBO9780511811685, <https://www.cambridge.org/core/books/multiple-view-geometry-in-computer-vision/0B6F289C78B2B23F596CAA76D3D43F7A>
23. Irschara, A., Zach, C., Frahm, J.M., Bischof, H.: From structure-from-motion point clouds to fast location recognition. In: 2009 IEEE Conference on Computer Vision and Pattern Recognition. pp. 2599–2606 (Jun 2009), DOI: 10.1109/CVPR.2009.5206587, iSSN: 1063-6919
24. Kristan, M., Matas, J., Leonardis, A., Vojíř, T., Pflugfelder, R., Fernandez, G., Nebehay, G., Porikli, F., Cehovin, L.: A Novel Performance Evaluation Methodology for Single-Target Trackers. IEEE Transactions on Pattern Analysis and Machine Intelligence (2016), DOI: 10.1109/TPAMI.2016.2516982
25. Laskar, Z., Melekhov, I., Kalia, S., Kannala, J.: Camera Relocalization by Computing Pairwise Relative Poses Using Convolutional Neural Network. In: 2017 IEEE International Conference on Computer Vision Workshop (ICCVW). pp. 920–929. IEEE Computer Society (Oct 2017), DOI: 10.1109/ICCVW.2017.113, <https://www.computer.org/csdl/proceedings-article/iccvw/2017/1034a920/120mNyLOTim>, iSSN: 2473-9944

26. Lee, D., Ryu, S., Yeon, S., Lee, Y., Kim, D., Han, C., Cabon, Y., Weinzaepfel, P., Guerin, N., Csurka, G., Humenberger, M.: Large-scale Localization Datasets in Crowded Indoor Spaces. In: 2021 IEEE/CVF Conference on Computer Vision and Pattern Recognition (CVPR). pp. 3226–3235. IEEE, Nashville, TN, USA (Jun 2021), DOI: 10.1109/CVPR46437.2021.00324, <https://ieeexplore.ieee.org/document/9578849/>
27. Lowe, D.G.: Distinctive Image Features from Scale-Invariant Keypoints. International Journal of Computer Vision **60**(2), 91–110 (Nov 2004), DOI: 10.1023/B:VISI.0000029664.99615.94, <http://link.springer.com/10.1023/B:VISI.0000029664.99615.94>
28. Ma, J., Jiang, X., Fan, A., Jiang, J., Yan, J.: Image Matching from Handcrafted to Deep Features: A Survey. International Journal of Computer Vision **129**(1), 23–79 (Jan 2021), DOI: 10.1007/s11263-020-01359-2
29. Macoir, N., Bauwens, J., Jooris, B., Van Herbruggen, B., Rossey, J., Hoebeke, J., De Poorter, E.: UWB Localization with Battery-Powered Wireless Backbone for Drone-Based Inventory Management. Sensors **19**(3), 467 (Jan 2019), DOI: 10.3390/s19030467, <https://www.mdpi.com/1424-8220/19/3/467>
30. Maddern, W., Pascoe, G., Linegar, C., Newman, P.: 1 year, 1000 km: The Oxford RobotCar dataset. International Journal of Robotics Research **36**(1), 3–15 (Jan 2017), DOI: 10.1177/0278364916679498
31. Maffra, F., Teixeira, L., Chen, Z., Chli, M.: Real-Time Wide-Baseline Place Recognition Using Depth Completion. IEEE Robotics and Automation Letters **4**(2), 1525–1532 (Apr 2019), DOI: 10.1109/LRA.2019.2895826
32. Maruyama, Y., Kato, S., Azumi, T.: Exploring the performance of ROS2. In: Proceedings of the 13th International Conference on Embedded Software. pp. 1–10. EMSOFT '16, Association for Computing Machinery, New York, NY, USA (Oct 2016), DOI: 10.1145/2968478.2968502
33. Masone, C., Caputo, B.: A Survey on Deep Visual Place Recognition. IEEE Access **9**, 19516–19547 (2021), DOI: 10.1109/ACCESS.2021.3054937
34. Michael, N., Mellinger, D., Lindsey, Q., Kumar, V.: The GRASP Multiple Micro-UAV Testbed. IEEE Robotics Automation Magazine **17**(3), 56–65 (Sep 2010), DOI: 10.1109/MRA.2010.937855
35. Milford, M.J., Wyeth, G.F.: SeqSLAM: Visual route-based navigation for sunny summer days and stormy winter nights. In: 2012 IEEE International Conference on Robotics and Automation. pp. 1643–1649 (May 2012), DOI: 10.1109/ICRA.2012.6224623, iSSN: 1050-4729
36. Moore, T., Stouch, D.: A Generalized Extended Kalman Filter Implementation for the Robot Operating System. In: Menegatti, E., Michael, N., Berns, K., Yamaguchi, H. (eds.) Intelligent Autonomous Systems 13. pp. 335–348. Advances in Intelligent Systems and Computing, Springer International Publishing, Cham (2016), DOI: 10.1007/978-3-319-08338-4_25
37. Naseer, T., Spinello, L., Burgard, W., Stachniss, C.: Robust visual robot localization across seasons using network flows. In: Proceedings of the Twenty-Eighth AAAI Conference on Artificial Intelligence. pp. 2564–2570. AAAI'14, AAAI Press, Québec City, Québec, Canada (2014)
38. Oleynikova, H., Burri, M., Lynen, S., Siegwart, R.: Real-time visual-inertial localization for aerial and ground robots. In: 2015 IEEE/RSJ International Conference on Intelligent Robots and Systems (IROS). pp. 3079–3085 (Sep 2015), DOI: 10.1109/IROS.2015.7353802

39. Paton, M., MacTavish, K., Warren, M., Barfoot, T.D.: Bridging the appearance gap: Multi-experience localization for long-term visual teach and repeat. In: 2016 IEEE/RSJ International Conference on Intelligent Robots and Systems (IROS). pp. 1918–1925 (Oct 2016), DOI: 10.1109/IROS.2016.7759303, iSSN: 2153-0866
40. Pfrunder, A., Borges, P.V.K., Romero, A.R., Catt, G., Elfes, A.: Real-time autonomous ground vehicle navigation in heterogeneous environments using a 3D LiDAR. In: 2017 IEEE/RSJ International Conference on Intelligent Robots and Systems (IROS). pp. 2601–2608 (Sep 2017), DOI: 10.1109/IROS.2017.8206083, iSSN: 2153-0866
41. Pless, R.: Using many cameras as one. In: 2003 IEEE Computer Society Conference on Computer Vision and Pattern Recognition, 2003. Proceedings. vol. 2, pp. II–587 (Jun 2003), DOI: 10.1109/CVPR.2003.1211520, iSSN: 1063-6919
42. Porav, H., Maddern, W., Newman, P.: Adversarial Training for Adverse Conditions: Robust Metric Localisation Using Appearance Transfer. In: 2018 IEEE International Conference on Robotics and Automation (ICRA). pp. 1011–1018 (May 2018), DOI: 10.1109/ICRA.2018.8462894, iSSN: 2577-087X
43. Rehrl, K., Gröchenig, S.: Evaluating Localization Accuracy of Automated Driving Systems. *Sensors* (Basel, Switzerland) **21**(17), 5855 (Aug 2021), DOI: 10.3390/s21175855, <https://www.ncbi.nlm.nih.gov/pmc/articles/PMC8433815/>
44. Revaud, J., Almazan, J., Rezende, R., Souza, C.D.: Learning With Average Precision: Training Image Retrieval With a Listwise Loss. In: 2019 IEEE/CVF International Conference on Computer Vision (ICCV). pp. 5106–5115. IEEE, Seoul, Korea (South) (Oct 2019), DOI: 10.1109/ICCV.2019.00521, <https://ieeexplore.ieee.org/document/9010047/>
45. Revaud, J., De Souza, C., Humenberger, M., Weinzaepfel, P.: R2D2: Reliable and Repeatable Detector and Descriptor. In: Advances in Neural Information Processing Systems. vol. 32. Curran Associates, Inc. (2019), <https://proceedings.neurips.cc/paper/2019/hash/3198dfd0aef271d22f7bcd6f12f5cb-Abstract.html>
46. Sarlin, P.E.: hloc - the hierarchical localization toolbox (Nov 2021), <https://github.com/cvg/Hierarchical-Localization>, original-date: 2020-07-16T07:25:35Z
47. Sarlin, P.E., Cadena, C., Siegwart, R., Dymczyk, M.: From Coarse to Fine: Robust Hierarchical Localization at Large Scale. In: 2019 IEEE/CVF Conference on Computer Vision and Pattern Recognition (CVPR). pp. 12708–12717. IEEE, Long Beach, CA, USA (Jun 2019), DOI: 10.1109/CVPR.2019.01300, <https://ieeexplore.ieee.org/document/8953492/>
48. Sarlin, P.E., DeTone, D., Malisiewicz, T., Rabinovich, A.: SuperGlue: Learning Feature Matching With Graph Neural Networks. In: 2020 IEEE/CVF Conference on Computer Vision and Pattern Recognition (CVPR). pp. 4937–4946. IEEE, Seattle, WA, USA (Jun 2020), DOI: 10.1109/CVPR42600.2020.00499, <https://ieeexplore.ieee.org/document/9157489/>
49. Sarlin, P.E., Unagar, A., Larsson, M., Germain, H., Toft, C., Larsson, V., Pollefeys, M., Lepetit, V., Hammarstrand, L., Kahl, F., Sattler, T.: Back to the Feature: Learning Robust Camera Localization from Pixels to Pose. In: 2021 IEEE/CVF Conference on Computer Vision and Pattern Recognition (CVPR). pp. 3246–3256. IEEE, Nashville, TN, USA (Jun 2021), DOI: 10.1109/CVPR46437.2021.00326, <https://ieeexplore.ieee.org/document/9577733/>
50. Sattler, T., Maddern, W., Toft, C., Torii, A., Hammarstrand, L., Stenborg, E., Safari, D., Okutomi, M., Pollefeys, M., Sivic, J., Kahl, F., Pajdla, T.: Benchmarking

6DOF Outdoor Visual Localization in Changing Conditions. In: 2018 IEEE/CVF Conference on Computer Vision and Pattern Recognition. pp. 8601–8610 (Jun 2018), DOI: 10.1109/CVPR.2018.00897, iSSN: 2575-7075

51. Schonberger, J.L., Frahm, J.M.: Structure-from-Motion Revisited. In: 2016 IEEE Conference on Computer Vision and Pattern Recognition (CVPR). pp. 4104–4113. IEEE, Las Vegas, NV, USA (Jun 2016), DOI: 10.1109/CVPR.2016.445, <http://ieeexplore.ieee.org/document/7780814/>
52. Schuster, M.J., Brand, C., Hirschmüller, H., Suppa, M., Beetz, M.: Multi-robot 6D graph SLAM connecting decoupled local reference filters. In: 2015 IEEE/RSJ International Conference on Intelligent Robots and Systems (IROS). pp. 5093–5100 (Sep 2015), DOI: 10.1109/IROS.2015.7354094
53. Schönberger, J.L., Zheng, E., Frahm, J.M., Pollefeys, M.: Pixelwise View Selection for Unstructured Multi-View Stereo. In: Leibe, B., Matas, J., Sebe, N., Welling, M. (eds.) Computer Vision – ECCV 2016. pp. 501–518. Lecture Notes in Computer Science, Springer International Publishing, Cham (2016), DOI: 10.1007/978-3-319-46487-9_31
54. Shotton, J., Glocker, B., Zach, C., Izadi, S., Criminisi, A., Fitzgibbon, A.: Scene Coordinate Regression Forests for Camera Relocalization in RGB-D Images. In: 2013 IEEE Conference on Computer Vision and Pattern Recognition. pp. 2930–2937. IEEE, Portland, OR, USA (Jun 2013), DOI: 10.1109/CVPR.2013.377, <http://ieeexplore.ieee.org/document/6619221/>
55. Stenborg, E., Sattler, T., Hammarstrand, L.: Using Image Sequences for Long-Term Visual Localization. In: 2020 International Conference on 3D Vision (3DV). pp. 938–948 (Nov 2020), DOI: 10.1109/3DV50981.2020.00104, iSSN: 2475-7888
56. Stumberg, L.v., Wenzel, P., Khan, Q., Cremers, D.: GN-Net: The Gauss-Newton Loss for Multi-Weather Relocalization. IEEE Robotics and Automation Letters (2020), DOI: 10.1109/LRA.2020.2965031
57. Utriainen, R., Pöllänen, M.: Review on mobility as a service in scientific publications. Research in Transportation Business & Management **27**, 15–23 (Jun 2018), DOI: 10.1016/j.rtbm.2018.10.005, <https://www.sciencedirect.com/science/article/pii/S2210539518300336>
58. Warren, M., Greeff, M., Patel, B., Collier, J., Schoellig, A.P., Barfoot, T.D.: There's No Place Like Home: Visual Teach and Repeat for Emergency Return of Multirotor UAVs During GPS Failure. IEEE Robotics and Automation Letters **4**(1), 161–168 (Jan 2019), DOI: 10.1109/LRA.2018.2883408
59. Zhang, X., Wang, L., Su, Y.: Visual place recognition: A survey from deep learning perspective. Pattern Recognition **113**, 107760 (May 2021), DOI: 10.1016/j.patcog.2020.107760, <https://www.sciencedirect.com/science/article/pii/S003132032030563X>

A Appendix

Tables 4 and 5 present the localization recall rates for all of the illumination conditions.

Table 4: Full table of recall rates for Town01

	<i>k</i> = 0	1	2	3	4	5
	.25 / .50 / 5.0	.25 / .50 / 5.0	.25 / .50 / 5.0	.25 / .50 / 5.0	.25 / .50 / 5.0	.25 / .50 / 5.0
	2 / 5 / 10	2 / 5 / 10	2 / 5 / 10	2 / 5 / 10	2 / 5 / 10	2 / 5 / 10
Ap-GeM	Sift	96.4 / 97.0 / 98.0	89.2 / 91.6 / 98.7	83.7 / 87.3 / 94.9	83.9 / 88.0 / 95.1	82.4 / 85.0 / 92.3
	D2-net	92.6 / 95.6 / 99.5	78.3 / 86.0 / 98.0	70.5 / 77.2 / 90.8	70.1 / 77.5 / 90.8	69.7 / 75.8 / 89.3
	R2D2	95.2 / 97.2 / 99.0	86.3 / 91.5 / 98.5	82.7 / 88.7 / 96.2	81.1 / 86.0 / 95.2	81.6 / 86.0 / 97.0
	SuperPoint	99.2 / 99.2 / 99.2	99.7 / 99.7 / 99.7	97.0 / 98.0 / 98.0	97.7 / 98.2 / 98.4	96.9 / 97.9 / 97.9
NetVLAD	Sift	95.7 / 97.2 / 99.0	88.2 / 92.4 / 99.0	87.0 / 91.3 / 98.0	86.3 / 90.0 / 97.4	85.9 / 90.0 / 96.2
	D2-net	94.1 / 95.9 / 99.8	79.1 / 84.9 / 97.2	68.8 / 77.0 / 91.2	69.1 / 75.9 / 88.2	69.7 / 76.3 / 89.3
	R2D2	94.4 / 96.9 / 99.8	85.1 / 91.3 / 99.2	81.0 / 87.4 / 97.4	81.5 / 87.6 / 96.9	80.5 / 86.0 / 96.6
	SuperPoint	99.8 / 99.8 / 99.8	99.5 / 99.8 / 99.8	99.3 / 99.7 / 98.7	99.5 / 99.7 / 98.5	99.2 / 99.5 / 97.9 / 98.9 / 99.3
	6	7	8	9	10	
	.25 / .50 / 5.0	.25 / .50 / 5.0	.25 / .50 / 5.0	.25 / .50 / 5.0	.25 / .50 / 5.0	.25 / .50 / 5.0
	2 / 5 / 10	2 / 5 / 10	2 / 5 / 10	2 / 5 / 10	2 / 5 / 10	2 / 5 / 10
	69.2 / 73.1 / 85.3	43.6 / 49.8 / 62.0	19.8 / 23.5 / 30.6	7.2 / 10.4 / 17.1	3.6 / 4.7 / 8.8	
	46.9 / 56.4 / 75.7	21.6 / 27.6 / 39.4	9.3 / 12.3 / 16.4	2.0 / 3.0 / 6.2	0.8 / 1.3 / 2.3	
	72.2 / 79.4 / 92.0	55.1 / 64.1 / 81.6	27.6 / 34.0 / 44.7	16.2 / 18.9 / 23.4	9.2 / 12.2 / 14.0	
	93.6 / 94.7 / 94.9	85.2 / 88.7 / 90.5	67.3 / 72.5 / 77.6	51.6 / 56.4 / 65.1	35.5 / 38.8 / 47.0	
	71.6 / 79.0 / 90.6	45.9 / 53.5 / 68.1	22.1 / 25.7 / 34.5	9.2 / 14.0 / 20.7	4.9 / 7.2 / 12.0	
	48.7 / 57.1 / 77.6	24.2 / 29.1 / 43.8	9.6 / 12.3 / 16.2	3.1 / 4.1 / 8.4	0.5 / 0.8 / 2.6	
	74.1 / 81.0 / 93.8	53.1 / 61.9 / 80.3	33.1 / 37.2 / 49.9	17.9 / 20.2 / 26.4	12.3 / 14.3 / 16.8	
	97.5 / 98.2 / 98.4	87.8 / 90.6 / 92.3	69.8 / 75.1 / 79.7	52.9 / 57.3 / 66.2	39.7 / 44.3 / 51.1	

Table 5: Full table of recall rates for Town10

	$k = 0$	1	2	3	4	5
	.25 / .50 / 5.0	.25 / .50 / 5.0	.25 / .50 / 5.0	.25 / .50 / 5.0	.25 / .50 / 5.0	.25 / .50 / 5.0
	2 / 5 / 10	2 / 5 / 10	2 / 5 / 10	2 / 5 / 10	2 / 5 / 10	2 / 5 / 10
Ap-GeM	Sift	94.4 / 98.4 / 99.6	94.0 / 94.4 / 94.8	89.6 / 91.2 / 92.8	87.3 / 88.9 / 90.9	90.1 / 91.3 / 93.3
	D2-net	98.0 / 99.6 / 100.	89.6 / 93.2 / 95.2	87.2 / 90.4 / 93.2	86.1 / 90.9 / 92.9	82.1 / 86.5 / 92.1
	R2D2	90.4 / 93.6 / 99.2	94.4 / 94.4 / 96.0	88.8 / 90.0 / 94.4	86.8 / 87.6 / 94.0	86.8 / 89.2 / 93.2
	SuperPoint	98.4 / 98.8 / 99.2	98.8 / 98.8 / 98.8	95.6 / 96.4 / 94.8	95.6 / 96.4 / 96.0	95.8 / 95.3 / 95.7
NetVLAD	Sift	94.9 / 97.2 / 98.8	96.8 / 97.2 / 97.2	94.4 / 94.8 / 96.0	90.5 / 92.9 / 94.8	88.8 / 90.8 / 92.4
	D2-net	97.2 / 99.2 / 100.	91.6 / 93.2 / 97.6	87.3 / 90.8 / 94.4	88.9 / 90.5 / 93.7	84.4 / 89.2 / 93.6
	R2D2	87.3 / 90.4 / 99.6	89.7 / 90.1 / 94.1	90.5 / 92.1 / 92.9	82.9 / 86.5 / 90.1	84.0 / 85.6 / 91.6
	SuperPoint	99.6 / 100. / 100.	98.8 / 98.8 / 98.8	98.0 / 98.0 / 98.0	98.4 / 98.8 / 98.8	98.8 / 97.6 / 97.6
	6	7	8	9	10	
	.25 / .50 / 5.0	.25 / .50 / 5.0	.25 / .50 / 5.0	.25 / .50 / 5.0	.25 / .50 / 5.0	.25 / .50 / 5.0
	2 / 5 / 10	2 / 5 / 10	2 / 5 / 10	2 / 5 / 10	2 / 5 / 10	2 / 5 / 10
	72.8 / 76.8 / 81.5	50.8 / 56.4 / 63.2	11.2 / 15.7 / 30.9	0.8 / 1.6 / 5.6	0.0 / 1.6 / 4.0	
	47.6 / 58.8 / 66.4	6.4 / 10.8 / 24.0	0.0 / 0.0 / 0.8	0.0 / 0.0 / 0.4	0.0 / 0.0 / 0.0	
	78.5 / 81.7 / 88.0	54.8 / 59.9 / 66.3	13.5 / 18.7 / 30.6	1.2 / 2.7 / 6.2	0.4 / 1.2 / 2.8	
	92.8 / 93.2 / 93.2	82.4 / 85.1 / 85.5	64.7 / 66.3 / 67.1	47.4 / 47.8 / 51.4	30.6 / 33.7 / 36.5	
	79.1 / 84.7 / 88.4	55.8 / 60.6 / 69.5	13.6 / 19.2 / 36.0	1.2 / 2.0 / 6.3	0.4 / 0.4 / 2.4	
	44.8 / 54.4 / 67.1	6.7 / 10.7 / 24.1	0.0 / 0.0 / 0.8	0.0 / 0.0 / 0.4	0.0 / 0.0 / 0.4	
	74.6 / 76.6 / 83.3	50.2 / 55.8 / 61.8	13.2 / 18.0 / 27.6	8.2 / 0.0 / 4.8	0.0 / 0.8 / 1.6	
	96.8 / 97.6 / 97.6	90.0 / 90.8 / 91.6	70.3 / 71.9 / 73.1	58.2 / 59.8 / 62.2	40.9 / 42.1 / 45.2	